

Data-driven Based Uncertainty Set Modeling Method for Microgrid Robust Optimization with Correlated Wind Power

Xinchen Li, Yixin Liu, *Member, IEEE*, Li Guo, *Member, IEEE*, Xialin Li, *Member, IEEE*,
and Chengshan Wang, *Senior Member, IEEE*

Abstract—Microgrid is considered an important part of the future zero carbon energy systems. However, the uncertainty caused by renewable energy source brings huge challenges to the scheduling of MG and restricts its ability of carbon emission reduction. In this paper, a novel improved multi-ellipsoidal uncertainty set modeling method is proposed to better depict the uncertainty of wind power and reduce the conservativeness of traditional robust optimization. Probabilistic information from historical data is utilized to capture the temporal correlation of forecast error of wind power, as well as the conditional correlation of forecast error with forecast value, making the uncertainty set more data-adaptive to variation of forecast results and more accurate for uncertainty description. A two-stage robust optimization model of a grid-connected microgrid is established based on the proposed uncertainty set and solved by column and constraint generation algorithm. Simulation results based on actual data illustrate the average unbalanced power of microgrid between day-ahead trading and real-time power exchange with utility grid is dropped by nearly 11.16% compared with a deterministic optimization method, 11.86% with traditional box uncertainty set-based robust optimization method, and 2.89% with stochastic optimization method.

Index Terms—Correlation, data driven, improved multi-ellipsoidal uncertainty set, microgrid robust optimization.

I. INTRODUCTION

BENEFITING from the advantages of renewable energy integration and management, microgrid (MG) has recently attracted substantial attention and is regarded as an important solution for zero-carbon transition of energy systems [1]. However, MG operation faces great challenges brought by renewable energy sources (RES) due to its intermittent and uncertain nature [2]. The way to deal with the uncertainty of RES has significant influence on system economy and reliability of MG, especially for day-ahead decision making process.

Stochastic optimization (SO) and robust optimization (RO) are considered the two most popular methods to tackle the uncertainty of RES. SO seeks for an optimal solution with expected minimum operation cost based on probability distribution of RES [3]. However, performance of SO depends on the accuracy of probability distribution of random variables, which is usually difficult to be precisely estimated with limited historical data. On the contrary, RO does not require an exact probability distribution, but uses an uncertainty set to describe the uncertainties of random variables and aims at finding the optimal solution for any realization of the given uncertainty set [4]. However, the solution provided by RO might be too conservative as it takes into account the worst scenario.

The uncertainty set determines the realization of random variables, thus has crucial influence on the robustness and conservativeness of RO model. From this point of view, many research studies have been carried out to reduce the conservativeness of RO by improving the uncertainty set. Different approaches for constructing uncertainty sets, including box uncertainty set (BUS), Polyhedral uncertain sets (PUS), and Ellipsoidal uncertainty sets (EUS) have been discussed in [5] based on historical data. The PUS is one of the most commonly used uncertainty sets since it has a linear boundary and is easy to be solved in RO problems. A general way to construct PUS is to add budget constraints in the form of BUS [6], [7]. The uncertainty set gets smaller than the original BUS with considering such constraints, making it less conservative while maintaining a similar robustness guarantee. For instance, a two-stage RO model was built in [8], conservativeness is regulated by choosing different uncertainty budgets according to the risk-averse level of MG operators. However, this kind of uncertainty set regards the uncertain information as independent variables, which may lead to a conservative solution when correlation exists. To this end, the correlation between neighboring wind farms was obtained through linear models based on the statistical data in [9]. A t -distribution was then established to construct a PUS with a certain confidence level to reduce the conservativeness. Reference [10] proposed a multi-band uncertainty set with higher resolution and modeled the spatial/temporal relationships of uncertainties among multiple narrower bands. Each band is assigned a weight coefficient reflecting its occurrence possibilities, which provides more flexibility for controlling solution conservativeness. Reference [11] expanded the multi-band

Manuscript received August 25, 2021; revised September 26, 2021; accepted November 9, 2021. Date of online publication August 18, 2022, date of current version February 28, 2023. This work was supported in part by the National Key R&D Program of China under Grant 2020YFB1506804 and the National Nature Science Foundation of China under Grant 51907140.

X. C. Li, Y. X. Liu (corresponding author, email: liuyixin@tju.edu.cn), L. Guo, X. L. Li, and C. S. Wang are with the Key Laboratory of Smart Grid of Ministry of Education, Tianjin University, Tianjin, 300072, China.

DOI: 10.17775/CSEEJPES.2021.06330

uncertainty set by considering linearized temporal correlation constraints of forecast errors of wind and load, which further reduces conservativeness by eliminating scenarios with lower probability. However, parameters such as the number of bands and the corresponding weight coefficients for formulating the multi-band uncertainty set are difficult to determine in practice.

The EUS shows better performance than PUS in terms of formulating the correlation among variables with smaller regions. In [12], the dynamic spatial correlations between wind farms were considered and an EUS was established based on observed wind generation measurements. The simulation results proved the advantages of EUS over PUS in conservativeness reduction. A minimum volume enclosing ellipsoid (MVEE) was employed as a convex hull to involve all the uncertain scenarios for an adjustable robust security constrained economic dispatch (SCED) model with wind power uncertainties in [13]. The SCED was cast as a second order cone programming (SOCP) problem and an inactive constraint reduction strategy was utilized to reduce the computational complexity. MVEE was also used in [14] to find the boundary of the region containing all historical scenarios, and a scaling factor was used to transform the EUS into PUS before conducting the economic dispatch of distribution networks with RES. Reference [15] applied EUS to address the spatial and temporal correlation of wind power, and utilized the affine policy to construct a robust transmission-constrained unit commitment model with adjustable conservatism. The analytical relationship between the budget value of the EUS and the actual probability of solution was given to guide the selection of budget value. While in [16], the EUS was used to capture the correlation between generation capacities and demands to address the transmission network expansion planning problem.

Recently, distributionally robust optimization (DRO) is proposed to overcome the shortcomings of traditional RO. The DRO extracts probabilistic information from historical data and construct an ambiguity set of probability distribution of uncertain variables. Then the decision is made considering the worst probability distribution [17]. Many approaches such as moment based [18], [19] and distance based [20], [21], are applied to formulate the ambiguity set. In [19], a family of wind power distributions was defined by an ambiguity set, and solution of the formulated two-stage DRO goes less conservative with more data. Reference [20] proposed a Wasserstein metric-based distributionally robust approximate framework, which has good computational efficiency in case of a large sample set. [21] utilized Kernel density estimation to construct ambiguous probability distributions of wind power and established a data-driven DRO model to dispatch energy and reserve.

Although the abovementioned literature carried out fruitful works on reducing conservativeness of RO, there exists a research gap that most studies ignore the correlation between forecast error and forecast value of RES power generation, which does exist in actual data. Fig. 1 shows the relationship between unified forecast error of wind power and forecast value from January 2019 to December 2019 provided by EIRGRID Group [22], where Fig. 1(a) presents the scatter

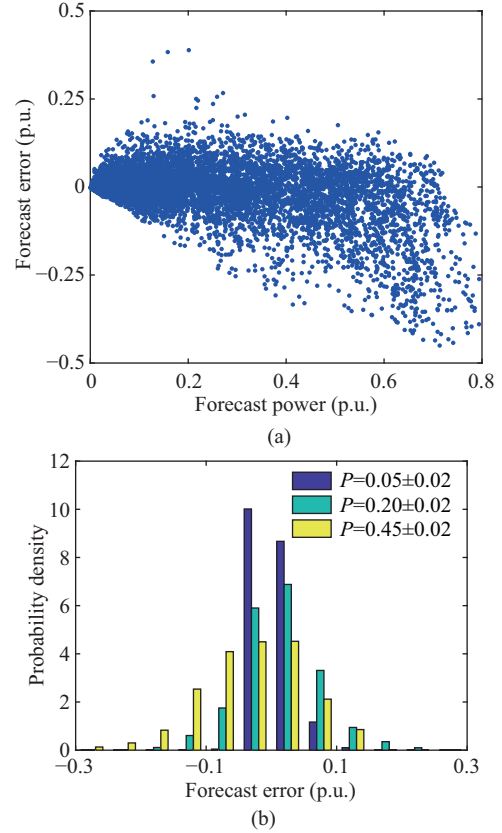


Fig. 1. Relationship between wind power forecast error and forecast value. (a) Scatter diagram of forecast error and forecast value. (b) Probability density of forecast error.

diagram of forecast error and forecast value and Fig. 1(b) demonstrates the probability density of forecast error under different forecast intervals. It can be observed that distribution of forecast error is more concentrated with smaller value in low forecast power situations, and becomes dispersed with greater error in high forecast power situation. This indicates that distribution characteristics of forecast error has correlation with the day-ahead forecast value, which needs to be considered to better capture the uncertainty.

To this end, this paper proposes a novel uncertainty set modeling method that is data-driven, based on a two-stage RO is established to address the day-ahead dispatch strategy for a grid-connected MG with wind power integrated. Compared with other modeling methods, the proposed method considers temporal and conditional correlation simultaneously, and optimizes the dimension of ellipsoid, as illustrated in Table I. The main work, as well as the contributions of this paper are demonstrated as follows:

- 1) The probabilistic information from historical data of

TABLE I
COMPARISON WITH OTHER UNCERTAINTY SET MODELING METHODS

Description	Proposed method	Traditional BUS	Traditional EUS	Traditional PUS
Temporal correlation	✓	×	✓	✓
Conditional correlation with forecast value	✓	×	×	
Dimension optimization	✓	×	×	×

forecast wind power and the corresponding forecast error is utilized to formulate an EUS based on conditional normal copula (CNC) method, which captures the temporal correlation of forecast error, as well as the conditional correlation of forecast error with the forecast value. Under this framework, the EUS can be updated based on the latest forecast power, thereby is more data-adaptive to the variation of forecast result.

2) An aggregate index is proposed to evaluate the overall performance and determine the optimal dimension of EUS via a rolling modeling method. The high-dimensional ellipsoid is then decomposed into multiple low-dimensional ellipsoids and combined with an improved BUS, which significantly reduces the conservativeness of the uncertainty set.

3) A two-stage RO model is built based on the improved multi-ellipsoidal uncertainty set (*i*-MEUS). The RO model is decomposed into a master problem (MP) and a subproblem (SP), where the MP is formulated as a mixed integer linear programming (MILP) problem and the SP is transformed to a mixed-integer second-order cone programming (MISOCP) problem via Binary Expansion (BE) and Big-M methods. The column and constraint generation (CC&G) algorithm is utilized to solve the two-stage RO model.

4) Numerous comparisons with deterministic optimization (DO), traditional BUS-based RO, improved BUS-based RO, EUS-based RO, and SO are conducted to verify the effectiveness of the proposed *i*-MEUS-based RO. Results show the proposed model is able to improve the economy of MG while maintaining robustness of the decision.

The rest of this paper is organized as follows: Section II presents the mathematical formulation of the proposed *i*-MEUS. Section III gives the two-stage RO model based on *i*-MEUS. Section IV details the solution procedure for optimal dimension of EUS, as well as the two-stage RO model. Case studies and simulation results are given and discussed in Section V, followed by the conclusion in Section VI.

II. DATA DRIVEN UNCERTAINTY SET MODELING

A. Conditional Normal Copula Modeling

Define $\mathbf{x} = [x_1, \dots, x_n]$ and $\mathbf{y} = [y_1, \dots, y_n]$ as the actual value and forecast value of wind power (WP), respectively; n denotes the dispatch cycle that is usually considered 24 in day-ahead decision making with time resolution of 1 hour. Define $\mathbf{e} = [e_1, \dots, e_n]$ as the corresponding forecast error that meets $\mathbf{x} = \mathbf{y} + \mathbf{e}$. The joint cumulative distribution of forecast error and forecast value is formulated as (1) according to normal copula theory [23]:

$$f_{\mathbf{e}, \mathbf{y}}(\mathbf{e}, \mathbf{y}) = \phi_{\mathbf{R}}(z_{x_1}, \dots, z_{x_n}, z_{y_1}, \dots, z_{y_n}) \prod_{i=1}^n f_{x_i}(e_i + y_i) f_{y_i}(y_i) \quad (1)$$

where $z_{x_i} = \Phi_0^{-1}[F_{x_i}(e_i + y_i)]$ and $z_{y_i} = \Phi_0^{-1}[F_{y_i}(y_i)]$ are intermediate variables of normal copula. $F(\cdot)$ denotes the cumulative distribution function (CDF) obtained from historical data of actual value and forecast value of WP. $\Phi_0^{-1}(\cdot)$ presents the inverse function of standard normal CDF of $\Phi_0(\cdot)$. $f(\cdot)$ indicates the probability density function (PDF). $\phi_{\mathbf{R}}(\cdot)$

means the PDF of standard multivariate normal distribution with covariance matrix of \mathbf{R} . Let $\mathbf{z}_x = [z_{x_1}, \dots, z_{x_n}]^T$, $\mathbf{z}_y = [z_{y_1}, \dots, z_{y_n}]^T$, and $\mathbf{z} = [\mathbf{z}_x^T, \mathbf{z}_y^T]^T$ obeys standard normal CDF, written as $\mathbf{z} \sim N(\mathbf{0}, \mathbf{R})$. Covariance matrix \mathbf{R} is calculated as:

$$\mathbf{R} = \begin{bmatrix} \mathbf{R}_{11} & \mathbf{R}_{12} \\ \mathbf{R}_{21} & \mathbf{R}_{22} \end{bmatrix} = \begin{bmatrix} \mathbf{R}_{xx} & \mathbf{R}_{xy} \\ \mathbf{R}_{yx} & \mathbf{R}_{yy} \end{bmatrix} \quad (2)$$

and

$$\mathbf{R}_{xy} = \begin{bmatrix} \rho(z_{x_1}, z_{y_1}) & \dots & \rho(z_{x_1}, z_{y_n}) \\ \vdots & \ddots & \vdots \\ \rho(z_{x_n}, z_{y_1}) & \dots & \rho(z_{x_n}, z_{y_n}) \end{bmatrix} \quad (3)$$

where $\rho(z_{x_i}, z_{y_i}) = 2 \sin[\rho_r(x_i, y_i)\pi/6]$. ρ and ρ_r are linear correlation coefficient and spearman correlation coefficient, respectively. \mathbf{R}_{xx} , \mathbf{R}_{yx} , and \mathbf{R}_{yy} can be calculated in the same way.

A conditional normal copula (CNC) model of forecast error is then formulated as:

$$\begin{aligned} f_{\mathbf{e}|\mathbf{y}}(\mathbf{e}|\mathbf{y}) &= f_{\mathbf{e}, \mathbf{y}}(\mathbf{e}, \mathbf{y}) / f_{\mathbf{y}}(\mathbf{y}) \\ &= \frac{\phi_{\mathbf{R}}(\mathbf{z}_x^T, \mathbf{z}_y^T)}{\phi_{\mathbf{R}_{yy}}(\mathbf{z}_y^T)} \prod_{i=1}^n f_{x_i}(e_i + y_i) \\ &= f_{\mathbf{z}_x|\mathbf{z}_y}(\mathbf{z}_x^T | \mathbf{z}_y^T) \prod_{i=1}^n f_{x_i}(e_i + y_i) \end{aligned} \quad (4)$$

where $\mathbf{z}_y \sim N(\mathbf{0}, \mathbf{R}_{yy})$. $\mathbf{z}_x|\mathbf{z}_y$ is the conditional distribution of multivariate normal distribution, which is essentially a multivariate normal distribution that meets $\mathbf{z}_x|\mathbf{z}_y \sim N(\boldsymbol{\mu}_{\mathbf{z}_x|\mathbf{z}_y}, \mathbf{R}_{\mathbf{z}_x|\mathbf{z}_y})$. According to the nature of conditional distribution of multivariate normal distribution, the expected value vector and covariance matrix can be obtained as follows [24]:

$$\begin{cases} \boldsymbol{\mu}_{\mathbf{z}_x|\mathbf{z}_y} = \mathbf{R}_{xy} \mathbf{R}_{yy}^{-1} \mathbf{z}_y \\ \mathbf{R}_{\mathbf{z}_x|\mathbf{z}_y} = \mathbf{R}_{xx} - \mathbf{R}_{xy} \mathbf{R}_{yy}^{-1} \mathbf{R}_{yx} \end{cases} \quad (5)$$

$\mathbf{z}_x|\mathbf{z}_y$ depicts the conditional correlation of the forecast value and actual value of WP, which enables us to generate numbers of WP samples denoting possible realization of WP in the next day based on the latest day-ahead forecast value. The detailed sampling process is illustrated as follows:

1) Establish marginal distribution of actual value and forecast value of WP in each time period based on historical data. Calculate the covariance matrix \mathbf{R} via (2) and (3);

2) Get $z_{y_i} = \Phi_0^{-1}[F_{y_i}(y_i)]$ according to the latest day-ahead forecast value;

3) Obtain the expected value and covariance matrix of $\mathbf{z}_x|\mathbf{z}_y$ based on (5);

4) Generate numbers of samples of \mathbf{z}_x by sampling $\mathbf{z}_x|\mathbf{z}_y$, and then the samples of actual value of WP can be obtained through $x_i = F_{x_i}^{-1}[\Phi_0(z_{x_i})]$;

The sample vector $\mathbf{x}_s = [x_1, \dots, x_n]^T$ achieved by the aforementioned sampling process considers not only temporal correlation, but also distribution characteristic of forecast error under different day-ahead forecast values, thus is more accurate in describing the uncertainty of WP due to its stronger data adaptive ability to the forecast results variation.

B. Formulation for Ellipsoidal Uncertainty Set

An ellipsoidal uncertainty set (EUS) with a given confidence level α_C is established to involve generated samples \mathbf{x}_s , which is formulated as:

$$(\mathbf{x}^{\text{EUS}} - \boldsymbol{\mu}_x)^T \mathbf{R}_x^{-1} (\mathbf{x}^{\text{EUS}} - \boldsymbol{\mu}_x) \leq C_\alpha \quad (6)$$

where $\boldsymbol{\mu}_x$ and \mathbf{R}_x are respectively, the expected value vector and covariance matrix of \mathbf{x}_s . C_α is a constant corresponding to α_C . Each sample \mathbf{x}_s is brought into (7) and the probability distribution of C can be achieved by considering all the samples. Let $\Pr\{C \leq C_\alpha\} = \alpha_C$ so we can get the value of C_α .

$$C = (\mathbf{x}_s - \boldsymbol{\mu}_x)^T \mathbf{R}_x^{-1} (\mathbf{x}_s - \boldsymbol{\mu}_x) \quad (7)$$

The center of EUS is up to $\boldsymbol{\mu}_x$ and shape is mainly influenced by \mathbf{R}_x . The covered region of EUS increases along with the increase of C_α , denoting that EUS is more likely to involve the possible realization of WP. However, the conservativeness goes stronger concomitantly as the invalid region of EUS may increase dramatically to involve the isolated samples.

C. Formulation for *i*-MEUS

The formulated uncertainty set in Section B is a high-dimensional EUS that considers the temporal correlation of n time periods of WP for day-ahead decision making. However, although a high-dimensional EUS is more likely to cover the actual realization of wind power, the weak correlation among distant time periods makes EUS too conservative due to its large volume. On the contrary, a low-dimensional EUS has smaller volume but may not involve enough wind power data. As a result, a trade-off between wind power coverage capacity and conservativeness should be made in an optimal manner. To this end, we decompose the high-dimensional EUS into several low-dimensional EUS by considering the strong correlation in adjacent time periods. Fig. 2 demonstrates the idea of high-dimensional ellipsoid decomposition. Suppose the correlation of T_R time periods is considered, R is the number of low-dimensional EUS and $R = n - T_R + 1$. The low-dimensional EUS will be created by rolling modeling the EUS via CNC method. For each EUS, the dimension is reduced from n to T_R , and the MEUS is the intersection of these R ellipsoids.

The r -th T_R -dimensional EUS, defined as $\Omega_{T_R,r}$, considers the temporal correlation among time interval $[r, r + T_R - 1]$, $1 \leq r \leq R$, and is used to involve possible realization of wind power among this time interval, which is expressed as:

$$\Omega_{T_R,r} = \left\{ \mathbf{x}_r^{\text{EUS}} \mid (\mathbf{x}_r^{\text{EUS}} - \boldsymbol{\mu}_{x,r})^T \mathbf{R}_{x,r}^{-1} (\mathbf{x}_r^{\text{EUS}} - \boldsymbol{\mu}_{x,r}) \leq C_{\alpha,r}, r = 1, \dots, R \right\} \quad (8)$$

Then the MEUS is formulated as:

$$\Omega_{\text{MEUS}} = \bigcap_{r=1}^R \Omega_{T_R,r} \quad (9)$$

The key point for MEUS modeling is to determine the optimal value of T_R that enables the MEUS to involve possible realization of WP with limited volume. To achieve this goal, an integrity index and an efficiency index are proposed. Define

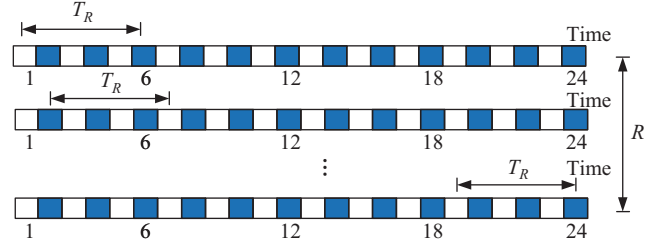


Fig. 2. Rolling modeling method for MEUS.

D as the number of days used to evaluate the performance of MEUS, and d denotes the day index. The two indexes are formulated as:

$$\zeta = \frac{1}{D} \sum_{d=1}^D \frac{N_d^{\max}}{n} \quad (10)$$

$$\eta = 1 - \frac{\lg\left(\frac{1}{D} \sum_{d=1}^D V_d^{\text{BUS} \cap \text{MEUS}}\right)}{\lg\left(\frac{1}{D} \sum_{d=1}^D V_d^{\text{BUS}}\right)} \quad (11)$$

In (10), N_d^{\max} indicates the maximum number of time periods that MEUS of day d can cover the actual value of WP in the same day. The integrity index ζ is defined as the average value of proportion of N_d^{\max} , so as to ensure more actual value of WP is involved in MEUS. In (11), the efficiency index η reflects the proportional relationship of the volume between the MEUS and a benchmark BUS. The BUS constructed in this paper also considers the conditional correlation of forecast error and forecast value in each time period, corresponding to a one-dimensional CNC model demonstrated in Section A. Therefore, the BUS is established based on the WP samples $\mathbf{x}_s^{\text{BUS}}$ generated by the one-dimensional CNC model, expressed as:

$$\Omega_{\text{BUS}} = \{x_i^{\text{BUS}} \mid x_i^{\text{BUS}} \in [b_{\text{LB},i}, b_{\text{UB},i}], i = 1, \dots, n\} \quad (12)$$

The lower limit $b_{\text{LB},i}$ and upper limit $b_{\text{UB},i}$ are obtained from the distribution of the samples $\mathbf{x}_s^{\text{BUS}}$ and (13) with confidence level of α_C :

$$\Pr(x_i^{\text{BUS}} \leq b_{\text{LB},i}) = \Pr(x_i^{\text{BUS}} \geq b_{\text{UB},i}) = 1 - \alpha_C/2 \quad (13)$$

In (11), V_d^{BUS} denotes the volume of BUS in day d . $V_d^{\text{BUS} \cap \text{MEUS}}$ represents the volume of intersection of BUS and MEUS in day d . The formulated efficiency index η , standardized within a range of [0, 1], can be used to evaluate the conservation of MEUS. The smaller the efficiency index is, the more conservative the set will be. Note it is difficult to obtain the precise volume of $V_d^{\text{BUS} \cap \text{MEUS}}$. Therefore, an approximate estimation method based on random discrete points is applied.

First, a large number of random points are generated in the BUS of day d , denoted as N_d^{BUS} . Then, the number of points belonging to the intersection of BUS and MEUS is recorded as $N_d^{\text{BUS} \cap \text{MEUS}}$. The approximate expression of the efficiency index is then formulated as:

$$\eta \approx 1 - \frac{\lg\left(\frac{1}{D} \sum_{d=1}^D N_d^{\text{BUS} \cap \text{MEUS}}\right)}{\lg\left(\frac{1}{D} \sum_{d=1}^D N_d^{\text{BUS}}\right)} \quad (14)$$

The MEUS would be more efficient with larger value of η , but also needs to consider the performance of ζ . Therefore, an aggregate index is established as:

$$\vartheta = a\zeta + (1-a)\eta \quad (15)$$

where a denotes the weight coefficient that is valued within (0, 1).

The value of T_R with best performance of aggregate index ϑ will be chosen as the solution. To further improve performance of the uncertainty set and overcome the shortcomings of MEUS in terms of over conservativeness caused by extreme scenarios included in the tail, an improved MEUS (i -MEUS) is finally constructed as the intersection of MEUS and BUS formulated as (9) and (12) respectively, i.e.:

$$\Omega_{i\text{-MEUS}} = \Omega_{\text{BUS}} \cap \Omega_{\text{MEUS}} \quad (16)$$

III. DAY-AHEAD TWO-STAGE RO MODEL

A typical grid-connected MG consists of controllable distributed generator (DG), wind turbine (WT), battery energy storage system (BESS), demand response load (DR), and conventional load is considered. In this paper, we extend the traditional RO model to an i -MEUS-based two-stage RO model to reduce the conservativeness, which is formulated as:

$$\min \left\{ \max \min \Delta t \left[\begin{array}{l} (a_{\text{DG}}P_{\text{DG},t} + b_{\text{DG}}) \\ + k_{\text{BESS}} \left(\frac{P_{\text{BESS},t}^{\text{dis}}}{\eta^{\text{dis}}} + P_{\text{BESS},t}^{\text{ch}} \eta^{\text{ch}} \right) \\ + k_{\text{DR}} |P_{\text{DR},t} - P_{\text{DR},t}^*| \\ + \pi_t (P_{\text{UG},t}^{\text{buy}} - P_{\text{UG},t}^{\text{sell}}) \end{array} \right] \right\} \quad (17)$$

subject to following constraints:

$$P_{\text{DG}}^{\min} \leq P_{\text{DG},t} \leq P_{\text{DG}}^{\max} \quad (18)$$

$$0 \leq P_{\text{BESS},t}^{\text{dis}} \leq B_{\text{BESS},t} P_{\text{BESS}}^{\text{dis,max}} \quad (19)$$

$$0 \leq P_{\text{BESS},t}^{\text{ch}} \leq (1 - B_{\text{BESS},t}) P_{\text{BESS}}^{\text{ch,max}} \quad (20)$$

$$\frac{1}{\eta^{\text{dis}}} \sum_{t=1}^n P_{\text{BESS},t}^{\text{dis}} \Delta t - \eta^{\text{ch}} \sum_{t=1}^n P_{\text{BESS},t}^{\text{ch}} \Delta t = 0 \quad (21)$$

$$E_{\text{BESS}}^{\min} \leq E_{\text{BESS},0} + \sum_{t=1}^t \left(P_{\text{BESS},t'}^{\text{ch}} \eta^{\text{ch}} - \frac{P_{\text{BESS},t'}^{\text{dis}}}{\eta^{\text{dis}}} \right) \Delta t \leq E_{\text{BESS}}^{\max} \quad (22)$$

$$\sum_{t=1}^n P_{\text{DR},t} \Delta t = E_{\text{DR}} \quad (23)$$

$$P_{\text{DR},t}^{\min} \leq P_{\text{DR},t} \leq P_{\text{DR},t}^{\max} \quad (24)$$

$$0 \leq P_{\text{UG},t}^{\text{buy}} \leq B_{\text{UG},t} P_{\text{UG}}^{\text{buy,max}} \quad (25)$$

$$0 \leq P_{\text{UG},t}^{\text{sell}} \leq (1 - B_{\text{UG},t}) P_{\text{UG}}^{\text{sell,max}} \quad (26)$$

$$P_{\text{UG},t}^{\text{buy}} + P_{\text{BESS},t}^{\text{dis}} + P_{\text{DG},t} + P_{\text{WT},t} = P_{\text{UG},t}^{\text{sell}} + P_{\text{DR},t} + P_{\text{BESS},t}^{\text{ch}} + P_{\text{L},t} \quad (27)$$

In (17), the objective is to minimize total day-ahead cost, including costs for dispatching the DG, BESS, and DR and cost of trading with utility grid (UG) for any realization of WP in $\Omega_{i\text{-MEUS}}$. Δt denotes the time resolution of the

optimization problem. $a_{\text{DG}}/b_{\text{DG}}$, k_{BESS} , and k_{DR} represent the cost coefficients of DG, BESS, and DR, respectively. $P_{\text{DG},t}$, $P_{\text{BESS},t}^{\text{dis}}/P_{\text{BESS},t}^{\text{ch}}$, $P_{\text{DR},t}$, and $P_{\text{UG},t}^{\text{buy}}/P_{\text{UG},t}^{\text{sell}}$ express the power generation of DG, discharge/charge power of BESS, actual power consumption of DR, and purchasing/selling power of MG from/to UG at time period t respectively. η^{dis} and η^{ch} indicate the discharge and charge efficiency of BESS. $P_{\text{DR},t}^*$ means the expected power consumption of DR at time period t . π_t presents the day-ahead time-of-use (TOU) price of the UG.

Output power of DG is constrained by (18). Constraint (19)–(22) give the operational constraints of BESS. The maximum discharge and charge power of BESS are limited by (19) and (20), where $B_{\text{BESS},t}$ denotes the binary variable that is equal to 1 if BESS is discharging, and equal to 0 otherwise; Constraint (21) guarantees the remaining capacity at the last time period is equal to the initial capacity $E_{\text{BESS},0}$; Constraint (22) ensures the remaining capacity of BESS at each time period within the upper bound E_{BESS}^{\max} and lower bound E_{BESS}^{\min} . DR loads can be shifted in time but need to consume a certain amount of energy within a given time, as demonstrated in (23); E_{DR} denotes the prescribed energy requirement of DR loads in a dispatching cycle; Constraint (24) shows the regulating range of DR at time period t . Constraint (25) and (26) express the trading power limit between MG and UG, $B_{\text{UG},t}$ is equal to 1 when MG purchases power from UG, and equal to 0 when MG sells power to UG. Power balance is realized by constrain (27), $P_{\text{WT},t}$ and $P_{\text{L},t}$ are the output power of WT and power demand of conventional load at time period t , respectively.

The absolute term in (17) denotes the influence of load management on users' comfort, which can be linearized as (28) by introducing auxiliary variables and associated constraints (29) and (30) as [8]:

$$k_{\text{DR}} |P_{\text{DR},t} - P_{\text{DR},t}^*| = k_{\text{DR}} (P_{\text{DR}1,t} + P_{\text{DR}2,t}) \quad (28)$$

$$P_{\text{DR},t} - P_{\text{DR},t}^* + P_{\text{DR}1,t} - P_{\text{DR}2,t} = 0 \quad (29)$$

$$P_{\text{DR}1,t} \geq 0, P_{\text{DR}2,t} \geq 0 \quad (30)$$

The compact form of the two-stage RO model is then formulated as:

$$\min_{\mathbf{x}^{\text{ro}}} \left\{ \max_{\mathbf{u} \in \Omega_{i\text{-MEUS}}} \min_{\mathbf{y}^{\text{ro}} \in \Psi(\mathbf{x}^{\text{ro}}, \mathbf{u})} \mathbf{c}^{\text{T}} \mathbf{y}^{\text{ro}} \right\} \quad (31)$$

subject to:

$$\mathbf{D} \mathbf{y}^{\text{ro}} \geq \mathbf{d}$$

$$\mathbf{K} \mathbf{y}^{\text{ro}} = \mathbf{k}$$

$$\mathbf{F} \mathbf{x}^{\text{ro}} + \mathbf{G} \mathbf{y}^{\text{ro}} \geq \mathbf{h}$$

$$\mathbf{Q} \mathbf{y}^{\text{ro}} + \mathbf{u} = \hat{\mathbf{u}}_{\text{L}}$$

$$\mathbf{y}^{\text{ro}} \geq \mathbf{0} \quad (32)$$

where superscript "ro" denotes variables related to RO problem. \mathbf{x}^{ro} and \mathbf{y}^{ro} represent the binary variable vector and continuous variables, expressed as (33). To simplify analysis, only the uncertainty of WP is considered. However, this simplification does not affect the ability of the proposed method to deal with a variety of uncertain variables. \mathbf{u} indicates the uncertain variable vector related to WP. $\Psi(\mathbf{x}^{\text{ro}}, \mathbf{u})$ is the

feasible region of \mathbf{y}^{ro} with fixed \mathbf{x}^{ro} and \mathbf{u} .

$$\begin{cases} \mathbf{x}^{\text{ro}} = [B_{\text{BESS},t}, B_{\text{UG},t}]^{\text{T}} \\ \mathbf{y}^{\text{ro}} = [P_{\text{DG},t}, P_{\text{BESS},t}^{\text{ch}}, P_{\text{BESS},t}^{\text{dis}}, P_{\text{DR},t}, \\ P_{\text{DR1},t}, P_{\text{DR2},t}, P_{\text{UG},t}^{\text{buy}}, P_{\text{UG},t}^{\text{sell}}]^{\text{T}} \\ t = 1, \dots, n \end{cases} \quad (33)$$

In (31) and (32), \mathbf{c} is coefficient column vector of objective function. \mathbf{D} , \mathbf{K} , \mathbf{F} , \mathbf{G} , and \mathbf{Q} are coefficient matrices of variables corresponding to the constraints. \mathbf{d} , \mathbf{k} , and \mathbf{h} are constant column vectors. $\hat{\mathbf{u}}_L$ denotes the forecast value of conventional load. The first line of (32) corresponds to constraints (18), (22), and (24); The second line indicates (21), (23), and (29); The third line involves (19), (20), (25), and (26); The fourth line denotes (27).

IV. SOLUTION APPROACH

A. Solution Procedure for Optimal Dimension of EUS

The BUS formulated in (12) can be regarded as a special case of T_R -dimensional EUS with $T_R = 1$. Therefore, T_R is an integer valued within the range of $[1, n]$. The enumeration method is used to determine the optimal T_R based on historical data. The solution procedure is summarized as follows:

Algorithm 1: Solution procedure for optimal value of T_R

- 1 Initialize $T_R = 1$, $d = 1$, set the parameter of α_C and a
 - 2 Obtain WP samples \mathbf{x}_s according to step 1)–step 4) of Section II-A
 - 3 **while** $T_R \leq n$ **do**
 - 4 **while** $d \leq D$ **do**
 - 5 Establish R T_R -dimensional EUS via (6)–(9), and obtain N_d^{max} , N_d^{BUS} , and $N_d^{\text{BUS} \cap \text{MEUS}}$ for day d
 - 6 $d = d + 1$
 - 7 **end**
 - 8 Calculate aggregate index by (10), (14), and (15)
 - 9 Record the value of aggregate index marked with T_R
 - 10 $T_R = T_R + 1$, $d = 1$
 - 11 **end**
 - 12 Select T_R with maximum aggregate index value
-

B. Solution Procedure for Two-stage RO Model

The two-stage RO model is solved by the C&CG algorithm [9], which decomposes the model into a master problem (MP) and a subproblem (SP), and then solves them iteratively. The formulation of the MP is expressed as:

$$\begin{aligned} \text{MP : } & \min_{\mathbf{x}^{\text{ro}}} \xi \\ \text{s.t. } & \xi \geq \mathbf{c}^{\text{T}} \mathbf{y}_l^{\text{ro}} \\ & \mathbf{D} \mathbf{y}_l^{\text{ro}} \geq \mathbf{d} \\ & \mathbf{K} \mathbf{y}_l^{\text{ro}} = \mathbf{k} \\ & \mathbf{F} \mathbf{x}^{\text{ro}} + \mathbf{G} \mathbf{y}_l^{\text{ro}} \geq \mathbf{h} \end{aligned}$$

$$\begin{aligned} \mathbf{Q} \mathbf{y}_l^{\text{ro}} + \mathbf{u}_l^* &= \hat{\mathbf{u}}_L \\ \mathbf{y}_l^{\text{ro}} &\geq \mathbf{0} \\ \forall l &\in \mathcal{O} \end{aligned} \quad (34)$$

where ξ is the auxiliary variable. \mathbf{y}_l^{ro} denotes new variables generated from the SP and added to the MP. \mathcal{O} is the index set for wind uncertainty scenarios l ; \mathbf{u}_l^* is the worst-case realization of WP, obtained from SP in the last iteration.

MP is a MILP problem that can be solved by mature software. With the solution of MP, the SP below is to find the worst-case realization of WP:

$$\begin{aligned} \text{SP : } & \max_{\mathbf{u} \in \Omega_{\xi, \text{MEUS}}} \min_{\mathbf{y}^{\text{ro}} \in \Psi(\mathbf{x}^{\text{ro}*}, \mathbf{u})} \mathbf{c}^{\text{T}} \mathbf{y}^{\text{ro}} \\ & \mathbf{D} \mathbf{y}^{\text{ro}} \geq \mathbf{d} \\ & \mathbf{K} \mathbf{y}^{\text{ro}} = \mathbf{k} \\ & \mathbf{F} \mathbf{x}^{\text{ro}*} + \mathbf{G} \mathbf{y}^{\text{ro}} \geq \mathbf{h} \\ & \mathbf{Q} \mathbf{y}^{\text{ro}} + \mathbf{u} = \hat{\mathbf{u}}_L \\ & \mathbf{y}^{\text{ro}} \geq \mathbf{0} \end{aligned} \quad (35)$$

The inner minimization problem of the SP is a linear problem, thus can be recast into the following single-level maximization problem based on strong duality theory:

$$\begin{aligned} & \max_{\mathbf{u}, \boldsymbol{\gamma}, \boldsymbol{\lambda}, \boldsymbol{\nu}, \boldsymbol{\pi}} \mathbf{d}^{\text{T}} \boldsymbol{\gamma} + \mathbf{k}^{\text{T}} \boldsymbol{\lambda} + (\mathbf{h} - \mathbf{F} \mathbf{x}^{\text{ro}*})^{\text{T}} \boldsymbol{\nu} + \hat{\mathbf{u}}_L^{\text{T}} \boldsymbol{\pi} - \mathbf{u}^{\text{T}} \boldsymbol{\pi} \\ \text{s.t. } & \mathbf{D}^{\text{T}} \boldsymbol{\gamma} + \mathbf{K}^{\text{T}} \boldsymbol{\lambda} + \mathbf{G}^{\text{T}} \boldsymbol{\nu} + \mathbf{Q}^{\text{T}} \boldsymbol{\pi} \leq \mathbf{c} \\ & \boldsymbol{\gamma} \geq \mathbf{0}, \boldsymbol{\nu} \geq \mathbf{0} \end{aligned} \quad (36)$$

where $\boldsymbol{\gamma}$, $\boldsymbol{\lambda}$, $\boldsymbol{\nu}$, and $\boldsymbol{\pi}$ are dual variable vectors for the constraints of the first line to fourth line of (35).

The bilinear term $\mathbf{u}^{\text{T}} \boldsymbol{\pi}$ in (36) brings challenges to solve the problem. In this paper, the Binary Expansion (BE) is used to linearize this term [25]. The dual variable vector $\boldsymbol{\pi}$ is expressed by BE as:

$$\pi_t \approx \pi_t^{\min} + \Delta \pi \sum_{i=i_1}^{i_n} 2^i b_{i,t} \quad (37)$$

where π_t^{\min} denotes the minimum value of π at time period t . $\Delta \pi$ is the step size. $b_{i,t}$ is a binary variable associated with the i -th exponential term in the BE expression. i_1 and i_n are integers defining minimum and maximum exponential orders.

The bilinear term $\mathbf{u}^{\text{T}} \boldsymbol{\pi}$ is therefore approximated as:

$$\mathbf{u}^{\text{T}} \boldsymbol{\pi} = \boldsymbol{\pi}_{\min}^{\text{T}} \mathbf{u} + \Delta \pi \sum_{i=i_1}^{i_n} \sum_{t=1}^n 2^i b_{i,t} u_t \quad (38)$$

where $\boldsymbol{\pi}_{\min}^{\text{T}} = [\pi_1^{\min}, \dots, \pi_n^{\min}]^{\text{T}}$ is a constant vector. u_t is an element of \mathbf{u} .

Formula (38) is further linearized by introducing auxiliary variable $\alpha_{i,t} = b_{i,t} u_t$ and Big-M method [26] as:

$$\begin{cases} \mathbf{u}^{\text{T}} \boldsymbol{\pi} = \boldsymbol{\pi}_{\min}^{\text{T}} \mathbf{u} + \mathbf{f}_{\alpha}^{\text{T}} \boldsymbol{\alpha} \\ 0 \leq \alpha_{i,t} \leq b_{i,t} M \\ u_t - (1 - b_{i,t}) M \leq \alpha_{i,t} \leq u_t \end{cases} \quad (39)$$

where $M \in \mathbb{R}^+$ is big enough. The variable $\boldsymbol{\alpha}$ and coefficient \mathbf{f}_{α} are vectors with $(i_n - i_1 + 1)n$ dimension, which are expressed as:

$$\begin{cases} \boldsymbol{\alpha} = [\alpha_{i_1,1}, \dots, \alpha_{i_n,1}, \alpha_{i_1,2}, \dots, \alpha_{i_n,2}, \dots, \\ \alpha_{i_1,n}, \dots, \alpha_{i_n,n}]^T \\ \mathbf{f}_\alpha = \Delta\pi \cdot [2^{i_1}, \dots, 2^{i_n}, 2^{i_1}, \dots, 2^{i_n}, \dots, 2^{i_1}, \dots, 2^{i_n}]^T \end{cases} \quad (40)$$

It is worth noting that dual variable $\boldsymbol{\pi}$ corresponds to the shadow price of MG, whose value is limited within a small range. As a result, it will not bring much computational burden by using BE.

The uncertain variable vector \mathbf{u} is bounded by the i -MEUS of (16), which also makes the model (36) difficult to be solved. Since $\mathbf{R}_{x,r}^{-1}$ in (8) is a symmetric positive-definite matrix with the Cholesky decomposition $\mathbf{R}_{x,r}^{-1} = \mathbf{L}_r^T \mathbf{L}_r$, (9) is transformed to the following second-order cone form by introducing a variable vector $\boldsymbol{\omega}_r$:

$$\Omega_{\text{MEUS}} := \begin{cases} u_t, t = 1, \dots, n \\ \sqrt{C_\alpha} \boldsymbol{\omega}_r = \mathbf{L}_r (\mathbf{u}_r - \boldsymbol{\mu}_{x,r}) \\ \|\boldsymbol{\omega}_r\|_2 \leq 1, r = 1, \dots, R \end{cases} \quad (41)$$

The SP is then cast into the following MISOCP problem:

$$\begin{aligned} & \max_{\mathbf{u}, \boldsymbol{\gamma}, \boldsymbol{\lambda}, \boldsymbol{\nu}, \boldsymbol{\pi}, \boldsymbol{\alpha}, \mathbf{b}, \mathbf{B}_u} \mathbf{d}^T \boldsymbol{\gamma} + \mathbf{k}^T \boldsymbol{\lambda} + (\mathbf{h} - \mathbf{F} \mathbf{x}^{\text{ro}*})^T \boldsymbol{\nu} + \hat{\mathbf{u}}_L^T \boldsymbol{\pi} \\ & \quad - \boldsymbol{\pi}_{\min}^T \mathbf{u} - \mathbf{f}_\alpha^T \boldsymbol{\alpha} \\ & \text{s.t. } \mathbf{D}^T \boldsymbol{\gamma} + \mathbf{K}^T \boldsymbol{\lambda} + \mathbf{G}^T \boldsymbol{\nu} + \mathbf{Q}^T \boldsymbol{\pi} \leq \mathbf{c} \\ & \quad \pi_t = \pi_t^{\min} + \Delta\pi \sum_{i=i_1}^{i_n} 2^i b_{i,t} \\ & \quad 0 \leq \alpha_{i,t} \leq b_{i,t} M \\ & \quad u_t - (1 - b_{i,t}) M \leq \alpha_{i,t} \leq u_t \\ & \quad \sqrt{C_\alpha} \boldsymbol{\omega}_r = \mathbf{L}_r (\mathbf{u}_r - \boldsymbol{\mu}_{x,r}) \\ & \quad \|\boldsymbol{\omega}_r\|_2 \leq 1 \\ & \quad b_{\text{LB},t} \leq u_t \leq b_{\text{UB},t} \\ & \quad u_t \geq B_{u,t} \hat{u}_{\text{WT},t} \\ & \quad \sum_{t=1}^n B_{u,t} \geq n - \Gamma \\ & \quad \boldsymbol{\gamma} \geq \mathbf{0}, \boldsymbol{\nu} \geq \mathbf{0} \\ & \quad t = 1, \dots, n, r = 1, \dots, R \end{aligned} \quad (42)$$

where $\hat{u}_{\text{WT},t}$ is the day-ahead forecast value of WP at time period t . $B_{u,t}$ is a binary variable associated with realization of WP. Γ denotes the uncertainty budget that used to regulate the robustness of decision making [6].

The procedure of the C&CG algorithm is conducted iteratively, which is demonstrated as follows:

V. CASE STUDY

The proposed method is tested by actual data from Ref. [22], where the CNC model is constructed by using four months data, and performance is tested by another two months data. All the models are solved by IBM ILOG CPLEX 12.6.3 with MATLAB R2013a.

A. Temporal Correlation Analysis of Wind Power

The conditional correlation of forecast error and forecast

Algorithm 2: Solution procedure for two-stage RO

- 1 Initialize worst scenario \mathbf{u}_l^* . Set the upper bound $UB = +\infty$, lower bound $LB = -\infty$, iterations index $l = 0$, $O \in \emptyset$, convergence error $\varepsilon = 0.01$.
- 2 **while** $UB - LB \geq \varepsilon$ **do**
- 3 Solve the MP (34) based on \mathbf{u}_l^* and derive the optimal solution $(\mathbf{x}_{l+1}^{\text{ro}*}, \xi_{l+1}^*, \mathbf{y}_1^{\text{ro}*}, \dots, \mathbf{y}_l^{\text{ro}*})$. Update $LB = \xi_{l+1}^*$.
- 4 Solve the SP (42) with $\mathbf{x}_{l+1}^{\text{ro}*}$, and get the optimal solution $(\mathbf{y}_{l+1}^{\text{ro}*}, \mathbf{u}_{l+1}^*)$, then update $UB = \min\{UB, \mathbf{c}^T \mathbf{y}_{l+1}^{\text{ro}*}\}$.
- 5 Create new variables $\mathbf{y}_{l+1}^{\text{ro}}$ and add corresponding new constraints given in (34) to **MP** ($l > 0$)
- 6 $l = l + 1$
- 7 **end**
- 8 Return $\mathbf{x}_{l+1}^{\text{ro}*}$ and $\mathbf{y}_{l+1}^{\text{ro}*}$

value of the testing data has been presented in Fig. 1. Here the lower triangular Scatter Matrix and marginal histogram of forecast error of wind power is provided in Fig. 3 to verify the necessity of considering temporal correlation. The marginal distribution of forecast error at each time period obeys normal distribution. Scatter plots represent joint distribution of forecast error among different time periods. It can be seen that joint distribution of adjacent time period centers at the diagonal of the axis, showing strong correlation. While it becomes dispersed with increase of time interval. Accordingly, considering the strong temporal correlation is a benefit to limit the invalid region of uncertainty set and reduce the conservativeness.

As demonstrated in Section II-C, the optimal dimension is determined by the aggregate index. Fig. 4 shows the value of aggregate index under different T_R . Weight coefficient a is set to 0.3, as the efficiency index usually has a significant impact on the conservativeness of uncertainty set. It shows the aggregate index increases with increase of T_R at the beginning, which is mainly dominated by the integrity index. However, it drops quickly once T_R is larger than 3. This is caused by the deterioration of performance of efficiency index, as a larger volume of uncertainty set is required with the increase of T_R . Therefore, the optimal dimension is determined as 3, and the MEUS consists of the intersection of 22 ellipsoid sets. Then, the i -MEUS is constructed by combining MEUS with the box uncertainty set formulated as (12).

B. Optimization Results of i -MEUS-based RO Model

The formulated two-stage RO model aims at minimizing the day-ahead cost of microgrid under the ‘‘worst scenario’’ of wind power. It is worth noting the final cost of microgrid includes two parts: the day-ahead cost and the balancing cost caused by the deviation of day-ahead trading and real-time power exchange with the utility grid. For a certain time period, if the purchasing power in real-time is larger than in day-ahead trading plan, the unbalanced power should be compensated by the microgrid with the real-time selling price of the utility grid. On the contrary, the microgrid is considered to sell power to the utility grid with the real-time purchasing price

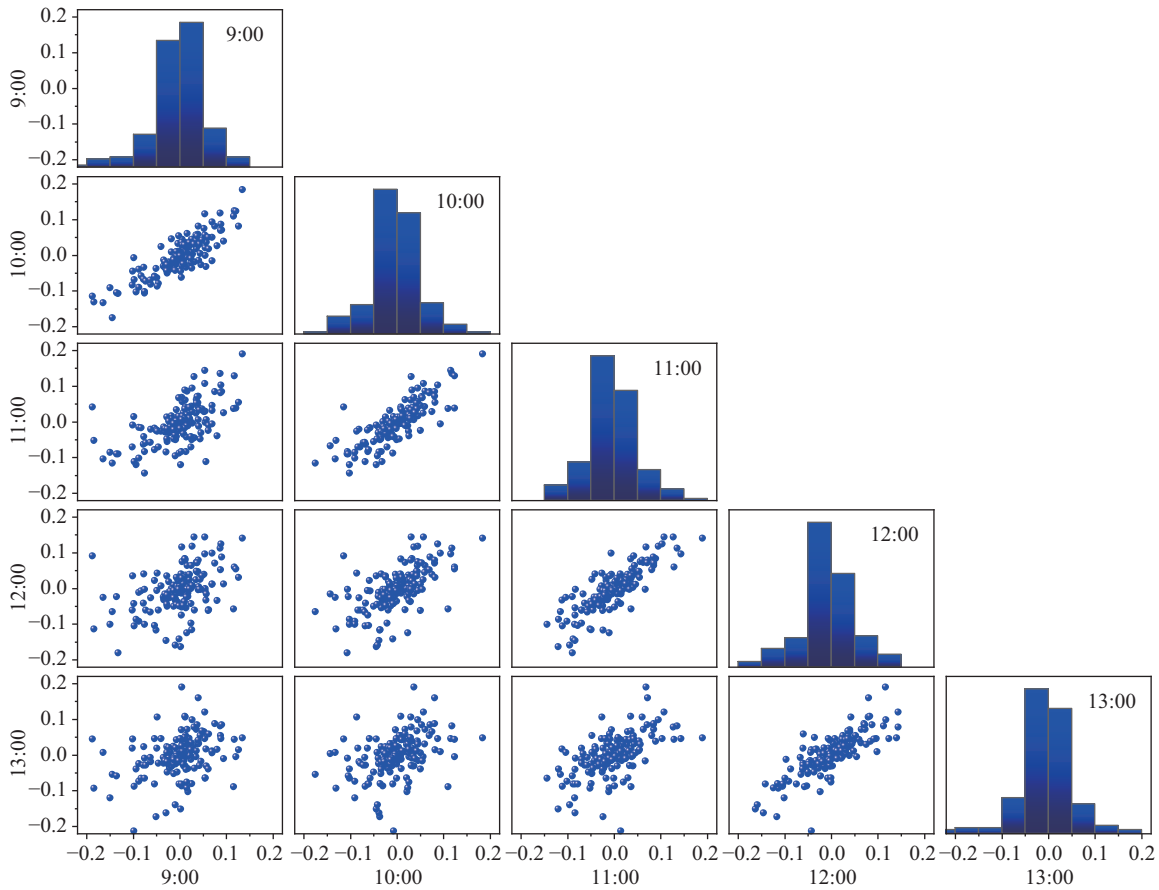


Fig. 3. Scatter plots and marginal histogram of forecast error.

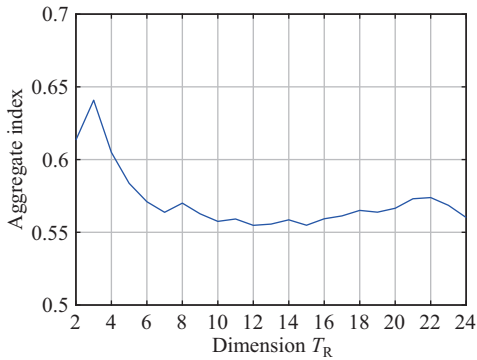


Fig. 4. Aggregate index with different T_R .

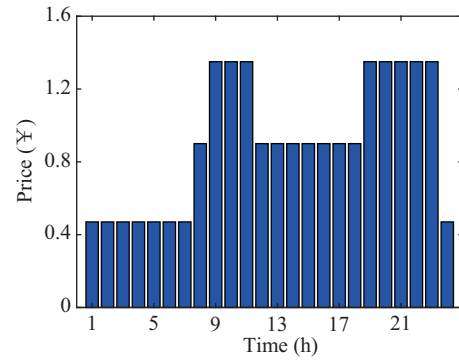


Fig. 5. Day-ahead time-of-use price of the utility grid.

if the purchasing power in real-time is lower than in day-ahead. Therefore, the optimization model should be evaluated according to overall performance in day-ahead and real time operation. In this section, only the day-ahead decision is analyzed, and the overall performance of the proposed method is discussed in Section C.

The operational and economic parameters of the microgrid can be found in [8]. The day-ahead time-of-use price of the utility grid is presented in Fig. 5. Fig. 6 demonstrates the dispatch scheme of DG and BESS. The positive value of BESS indicates discharging, and negative value denotes charging. The BESS is utilized to transport electricity from

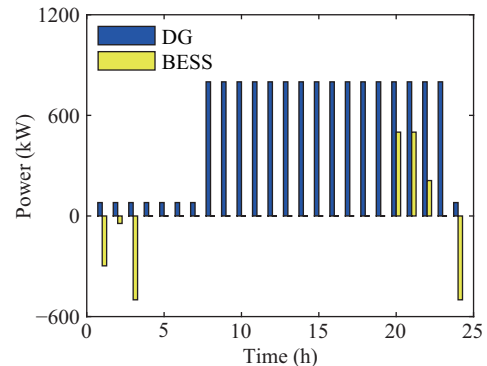


Fig. 6. Day-ahead dispatch of DG and BESS.

low price periods (1 h–3 h, 24 h) to high price periods (20 h–22 h), thus reducing day-ahead cost. The DG operates with minimum output power in 1 h–7 h and 24 h, as the day-ahead prices during these periods are lower than unit generation cost (¥0.47/kWh VS ¥0.67/kWh). While in the other periods, DG exports as much power as possible to reduce the cost of microgrid. Fig. 7 illustrates actual power consumption and expected power consumption of DR. Electricity demands of 19 h–21 h and 23 h are shifted to 1 h–7 h and 24 h to reduce cost while meeting the constraint of (23). Results indicate the rationality of the day-ahead decision made through the *i*-MEUS-based two-stage RO model.

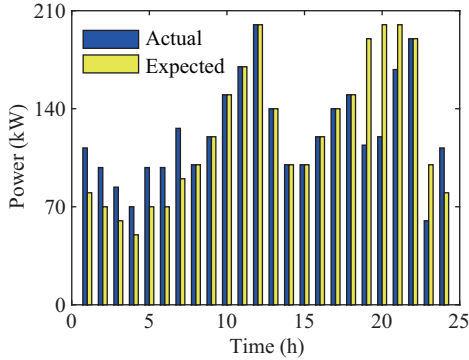


Fig. 7. The actual/expected power consumption of DR.

C. Comparison of Different Optimization Methods

It is clear the day-ahead decision has great influence on MG economy. Although balancing cost may be reduced with a conservative day-ahead decision, it always leads to a higher day-ahead cost and is uneconomic when considering both the day-ahead and balancing costs. Therefore, an accurate uncertainty modeling is required for the MG day-ahead decision making. In this Section, six optimization models are compared to verify the advantages of the proposed *i*-MEUS, which are demonstrated as:

1) Deterministic optimization model (DO), where no uncertainty is considered and wind power is equal to the forecast value.

2) BUS-based RO: the RO model of (31)–(32) is utilized, but the uncertainty set is replaced by a traditional BUS used in [8].

3) *i*-BUS-based RO: the RO model of (31)–(32) is utilized, but the uncertainty set is replaced by an improved BUS (*i*-BUS) defined in (12)–(13), i.e. the conditional correlation of forecast error and forecast value in each time period is considered.

4) EUS-based RO: the RO model of (31)–(32) is utilized, but the uncertainty set is replaced by an EUS defined as (8) with T_R valued as 24.

5) *i*-MEUS-based RO model proposed in this paper.

6) Stochastic optimization model (SO): the comparative SO model also considers the temporal correlation and the conditional correlation. The wind power samples are generated in the same way with *i*-MEUS-based RO model. Then, the *k*-means cluster method is used to reduce scenarios number according to the sum of square error (SSE) [27].

Figure 8 illustrates the relationship of SSE with cluster number. It can be seen that SSE reduces along with increase of scenarios number, and descending speed becomes very slow when the number is greater than 10. Therefore, ten scenarios are considered.

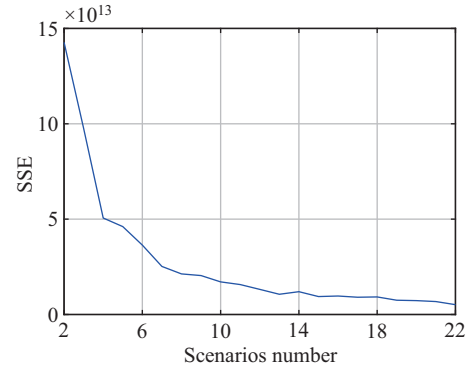


Fig. 8. SSE with different scenarios number.

Purchasing/selling prices of the utility grid in the real-time power market are usually lower/higher than in the day-ahead market [28]. Therefore, real-time purchasing price and selling price of utility grid are assumed to be 0.5 times and 1.5 times the day-ahead price at the corresponding periods, respectively [8]. Fig. 9 demonstrates performance of the six models in terms of day-ahead cost, balancing cost, total cost, day-ahead purchasing electricity, day-ahead selling electricity, and balancing electricity of the MG. All results are the daily average of test data. Balancing electricity means the sum of absolute value of surplus power and power gap in each period of MG in real time operation. As no uncertainty risk is considered in DO, day-ahead purchasing electricity is the lowest and the day-ahead selling electricity is the highest. Therefore, the DO makes a decision that is “ideal” with lowest day-ahead cost (¥1962). However, this day-ahead decision leads to a huge power gap that needs to be compensated by the MG to the utility grid, causing highest balancing cost (¥1374). When uncertainty is considered in the other five models, purchasing electricity goes higher and selling electricity goes lower in day-ahead decisions with different variation characteristics. Among the uncertain optimization models, the EUS-based RO model shows the strongest conservativeness. Although balancing cost is the lowest (¥393) due to large income from the utility grid for surplus power, the overall performance is the worst due to highest day-ahead cost (¥3122). This is caused by the weak correlation among distant time periods, which significantly increases the volume of EUS.

Simulation results also reveal the shortcoming of “over conservative” of traditional BUS-based robust method. The total costs of BUS-based RO model and *i*-BUS-based RO model are slightly higher than the DO model under the testing data (increased by 0.42% and 0.12%, respectively). The performance of *i*-BUS-based RO model is slightly better than the BUS-based RO model, which benefits from the consideration of conditional correlation. The improved BUS is updated based on the latest forecast value, improving

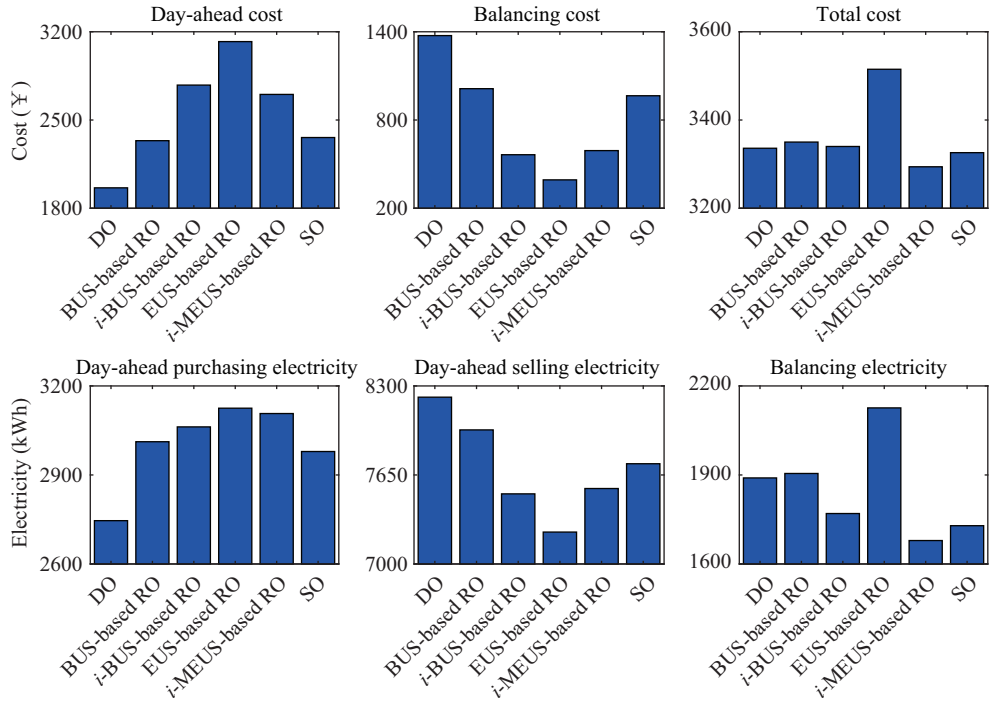


Fig. 9. Daily average results of different models.

accuracy of uncertainty modeling. The SO model achieves a relatively balanced solution in aspects of the day-ahead cost and balancing cost, showing better performance than the DO, BUS-based RO, *i*-BUS-based RO, and EUS-based RO. The total cost of SO model is reduced by 0.30% compared with the DO model under the testing data. Compared with the SO model, the proposed *i*-MEUS-based RO performs better in terms of balancing cost, as well as balancing electricity, thus has the lowest total cost among all the six models (reduced by 1.26% VS DO model).

The daily average value of balancing electricity of the six models are demonstrated in Table II. It can be seen the proposed *i*-MEUS-based RO model reduces the daily average balancing electricity by 11.16%, 11.86%, 5.14%, 21.03%, and 2.89% compared with the DO, BUS-based RO, *i*-BUS-based RO, EUS-based RO, and SO, respectively. Accordingly, overall performance is the best among the comparative models. Results denote the proposed method can reduce the conservativeness of traditional RO methods and improve accuracy for uncertainty modeling, realizing a balance between economy and robustness for the MG day-ahead decision making.

To better present the advantages of the proposed model, one day from the testing two months is selected for specific explanation. Wind power realization of DO, *i*-BUS-based RO, SO, and the proposed *i*-MEUS-based RO in day-ahead decision making is illustrated in Fig. 10. The corresponding

unbalanced power of each time period is provided in Fig. 11.

In Fig. 10, wind power realization of SO indicates the expected value of the 10 scenarios. It can be seen that wind power realization of DO model has large deviation with actual

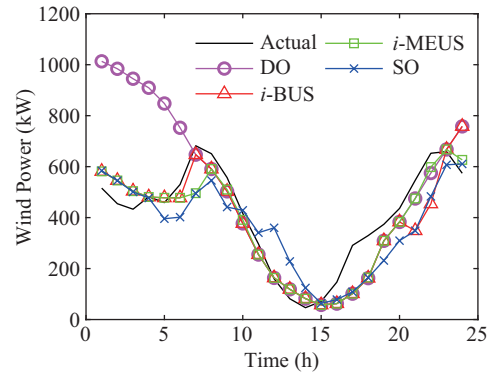


Fig. 10. Wind power realization of different models.

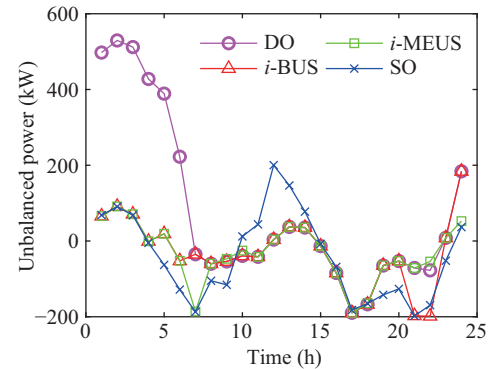


Fig. 11. Unbalanced power of different models.

TABLE II
BALANCING ELECTRICITY OF DIFFERENT MODELS

Method	Mean	Method	Mean
DO (kWh)	1890	EUS-based RO (kWh)	2126
BUS-based RO (kWh)	1905	<i>i</i> -MEUS-based RO (kWh)	1679
<i>i</i> -BUS-based RO (kWh)	1770	SO (kWh)	1729

wind power in 1 h–6 h, leading to large unbalanced power that needs to be compensated in Fig. 11. In the other time periods, deviation is limited within a small range, denoting good prediction accuracy of the testing data. Comparing the i -BUS-based RO with the proposed model, the main difference is that wind power realization at 21 h is selected as an independent worse scenario in i -BUS-based RO. While the proposed model prefers to select continuous periods as worse scenarios due to the temporal correlation, which reduces the unbalanced power as shown in Fig. 11 and improves uncertain modeling accuracy. When compared with the SO, the proposed model also performs better in many time periods, such as 5 h–6 h, 8 h–14 h, and 19 h–23 h.

In order to quantitatively compare the effectiveness of models, indexes such as correlation coefficient (CC), root mean square error (RMSE), Bias, mean absolute error (MAE), normalized root mean square error (NRMSE) and scatter index (SI) are utilized and presented in Table III. These indexes are formulated as (43)–(48), where $P_{WD,t}^{\text{actu}}$ and u_t represent the actual value of WP and realization of WP at time period t . $\bar{P}_{WD}^{\text{actu}}$ and \bar{u} are their average values, respectively. The range of CC is 0–1, and correlation is higher when the value is larger. RMSE, Bias, MAE and NRMSE are error evaluation indexes from different perspectives. SI indicates relative dispersion degree of the error. Fluctuation of error deviation is smaller when SI is smaller. It is obvious the proposed model has higher CC, smaller errors and smaller SI, which shows excellent performance in each aspect.

$$CC = \frac{\sum_{t=1}^n (P_{WD,t}^{\text{actu}} - \bar{P}_{WD}^{\text{actu}})(u_t - \bar{u})}{\sqrt{\sum_{t=1}^n (P_{WD,t}^{\text{actu}} - \bar{P}_{WD}^{\text{actu}})^2 \sum_{t=1}^n (u_t - \bar{u})^2}} \quad (43)$$

$$RMSE = \sqrt{\frac{1}{n} \sum_{t=1}^n (u_t - P_{WD,t}^{\text{actu}})^2} \quad (44)$$

$$Bias = \bar{u} - \bar{P}_{WD}^{\text{actu}} \quad (45)$$

$$MAE = \frac{1}{n} \sum_{t=1}^n |u_t - P_{WD,t}^{\text{actu}}| \quad (46)$$

$$NRMSE = \sqrt{\frac{\sum_{t=1}^n (u_t - P_{WD,t}^{\text{actu}})^2}{\sum_{t=1}^n (P_{WD,t}^{\text{actu}})^2}} \quad (47)$$

$$SI = \sqrt{\frac{\sum_{t=1}^n \left(\left(\frac{P_{WD,t}^{\text{actu}} - \bar{P}_{WD}^{\text{actu}}}{P_{WD,t}^{\text{actu}}} - (u_t - \bar{u}) \right)^2 \right)}{\sum_{t=1}^n (P_{WD,t}^{\text{actu}})^2}} \quad (48)$$

We also vary the sample size of wind power to further test performance of different optimization models. Total costs with different sample sizes are presented in Fig. 12. Total cost of DO remains unchanged as it does not require the data to train. As more data are considered, the EUS becomes larger with higher cost obtained by EUS-based RO model. The costs of BUS-based RO and i -BUS-based RO also increase slightly with increase of sample size. The cost of the proposed model almost remains the same under different sample sizes. Whereas

TABLE III
INDEXES OF WIND POWER REALIZATION OF DIFFERENT MODELS

Index	DO	i -BUS-based RO	i -MEUS-based RO	SO
CC	0.728	0.897	0.928	0.814
RMSE	233.684	96.805	80.203	119.069
Bias	79.010	-30.657	-30.188	-40.465
MAE	158.240	73.619	62.190	102.457
NRMSE	0.516	0.214	0.177	0.263
SI	0.486	0.203	0.164	0.247

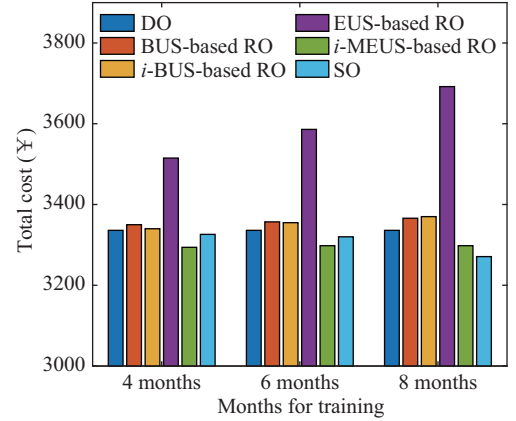


Fig. 12. Total costs of different models under different sample sizes.

the total cost of SO reduces when more data is used to generate scenarios, and it performs better than the proposed model when there has enough training data.

VI. CONCLUSION

Future zero carbon energy systems are integrated with large scale of RES, and MG plays an important role in increasing renewable energy penetration. This paper proposes an i -MEUS modeling method to address uncertainty brought by RES and reduce the conservativeness of robust optimization. The efficiency of the proposed model is verified using numerous cases, which shows that:

1) The proposed method has higher accuracy for uncertainty modeling. The day-ahead decision made by the proposed model is robust and less conservative. Average unbalanced power is reduced by 11.16%, 11.86%, 5.14%, 21.03%, and 2.89% as compared with the DO, BUS-based RO, i -BUS-based RO, EUS-based RO, and SO, respectively.

2) The proposed model shows better adaptability for limited historical data than the SO. Performance of the proposed model is satisfactory in the case of less training data. Therefore, it is more suitable for uncertain optimization problems with limited historical data.

Future work will focus on comparison with the DRO method that also utilizes probabilistic information of historical data, and try to combine the advantages of the two methods to further reduce conservativeness of RO.

REFERENCES

- [1] M. Yousif, Q. Ai, Y. Gao, W. A. Wattoo, Z. Q. Jiang, and R. Hao, "An optimal dispatch strategy for distributed microgrids using PSO," *CSEE Journal of Power and Energy Systems*, vol. 6, no. 3, pp. 724–734, Sep. 2020.

- [2] G. D. Liu, T. Jiang, T. B. Ollis, X. Li, F. X. Li, and K. Tomsovic, "Resilient distribution system leveraging distributed generation and microgrids: A review," *IET Energy Systems Integration*, vol. 2, no. 4, pp. 289–304, Dec. 2020.
- [3] Y. T. Lin, T. Y. Ji, Y. Z. Jiang, and Q. H. Wu, "Stochastic economic dispatch considering the dependence of multiple wind farms using multivariate Gaussian kernel copula," *CSEE Journal of Power and Energy Systems*, vol. 8, no. 5, pp. 1352–1362, Sep. 2022.
- [4] Q. Li, Y. B. Qiu, H. Q. Yang, Y. Xu, W. R. Chen, and P. Wang, "Stability-constrained two-stage robust optimization for integrated hydrogen hybrid energy system," *CSEE Journal of Power and Energy Systems*, vol. 7, no. 1, pp. 162–171, Jan. 2021.
- [5] Y. P. Guan and J. H. Wang, "Uncertainty sets for robust unit commitment," *IEEE Transactions on Power Systems*, vol. 29, no. 3, pp. 1439–1440, May 2014.
- [6] D. Bertsimas and M. Sim, "The price of robustness," *Operations Research*, vol. 52, no. 1, pp. 35–53, Feb. 2004.
- [7] A. Jalilvand-Nejad, R. Shafaei, and H. Shahriari, "Robust optimization under correlated polyhedral uncertainty set," *Computers & Industrial Engineering*, vol. 92, pp. 82–94, Feb. 2016.
- [8] Y. X. Liu, L. Guo, and C. S. Wang, "A robust operation-based scheduling optimization for smart distribution networks with multi-microgrids," *Applied Energy*, vol. 228, pp. 130–140, Oct. 2018.
- [9] J. Tan, Q. W. Wu, Q. R. Hu, W. Wei, and F. Liu, "Adaptive robust energy and reserve co-optimization of integrated electricity and heating system considering wind uncertainty," *Applied Energy*, vol. 260, pp. 114230, Feb. 2020.
- [10] C. X. Dai, L. Wu, and H. Y. Wu, "A multi-band uncertainty set based robust SCUC with spatial and temporal budget constraints," *IEEE Transactions on Power Systems*, vol. 31, no. 6, pp. 4988–5000, Nov. 2016.
- [11] Y. B. Chen, Z. Zhang, H. Chen, and H. P. Zheng, "Robust UC model based on multi-band uncertainty set considering the temporal correlation of wind/load prediction errors," *IET Generation, Transmission & Distribution*, vol. 14, no. 2, pp. 180–190, Jan. 2020.
- [12] P. Li, X. H. Guan, J. Wu, and X. X. Zhou, "Modeling dynamic spatial correlations of geographically distributed wind farms and constructing ellipsoidal uncertainty sets for optimization-based generation scheduling," *IEEE Transactions on Sustainable Energy*, vol. 6, no. 4, pp. 1594–1605, Oct. 2015.
- [13] T. Ding, J. J. Lv, R. Bo, Z. H. Bie, and F. X. Li, "Lift-and-project MVEE based convex hull for robust SCED with wind power integration using historical data-driven modeling approach," *Renewable Energy*, vol. 92, pp. 415–427, Jul. 2016.
- [14] Y. P. Zhang, X. M. Ai, J. Y. Wen, J. K. Fang, and H. B. He, "Data-adaptive robust optimization method for the economic dispatch of active distribution networks," *IEEE Transactions on Smart Grid*, vol. 10, no. 4, pp. 3791–3800, Jul. 2019.
- [15] Y. Tian, W. Wu, K. Y. Wang, Y. Fu, and G. J. Li, "Robust transmission constrained unit commitment under wind power uncertainty with adjustable conservatism," *IET Generation, Transmission & Distribution*, vol. 14, no. 5, pp. 824–832, Mar. 2020.
- [16] C. Roldán, R. Mínguez, R. García-Bertrand, and J. M. Arroyo, "Robust transmission network expansion planning under correlated uncertainty," *IEEE Transactions on Power Systems*, vol. 34, no. 3, pp. 2071–2082, May 2019.
- [17] H. J. Gao, Z. Y. Liu, Y. B. Liu, L. F. Wang, and J. Y. Liu, "A data-driven distributionally robust operational model for urban integrated energy systems," *CSEE Journal of Power and Energy Systems*, vol. 8, no. 3, pp. 789–800, May 2022.
- [18] J. X. Cao, B. Yang, S. Y. Zhu, C. Ning, and X. P. Guan, "Day-ahead chance-constrained energy management of energy hubs: a distributionally robust approach," *CSEE Journal of Power and Energy Systems*, vol. 8, no. 3, pp. 812–825, May 2022.
- [19] Y. Chen, W. Wei, F. Liu, and S. W. Mei, "Distributionally robust hydro-thermal-wind economic dispatch," *Applied Energy*, vol. 173, pp. 511–519, Jul. 2016.
- [20] R. J. Zhu, H. Wei, and X. Q. Bai, "Wasserstein metric based distributionally robust approximate framework for unit commitment," *IEEE Transactions on Power Systems*, vol. 34, no. 4, pp. 2991–3001, Jul. 2019.
- [21] X. Y. Xu, Z. Yan, M. Shahidehpour, Z. Y. Li, M. Y. Yan, and X. R. Kong, "Data-driven risk-averse two-stage optimal stochastic scheduling of energy and reserve with correlated wind power," *IEEE Transactions on Sustainable Energy*, vol. 11, no. 1, pp. 436–447, Jan. 2020.
- [22] EIRGRID Group. [Online]. Available: <http://www.eirgridgroup.com/how-the-grid-works/system-information/>
- [23] N. Zhang, C. Q. Kang, Q. Xia, and J. Liang, "Modeling conditional forecast error for wind power in generation scheduling," *IEEE Transactions on Power Systems*, vol. 29, no. 3, pp. 1316–1324, May 2014.
- [24] A. Jamalizadeh and N. Balakrishnan, "Conditional distributions of multivariate normal mean–variance mixtures," *Statistics & Probability Letters*, vol. 145, pp. 312–316, Feb. 2019.
- [25] H. X. Ye, J. H. Wang, and Z. Y. Li, "MIP reformulation for max-min problems in two-stage robust SCUC," *IEEE Transactions on Power Systems*, vol. 32, no. 2, pp. 1237–1247, Mar. 2017.
- [26] M. S. Bazaraa and J. J. Jarvis, *Linear Programming and Network Flows*, New York: Wiley, 1977, pp. 165–173.
- [27] M. A. Syakur, B. K. Khotimah, E. M. S. Rochman, and B. D. Satoto, "Integration K-means clustering method and elbow method for identification of the best customer profile cluster," *IOP Conference Series: Materials Science and Engineering*, vol. 336, pp. 012017, 2018.
- [28] G. D. Liu, Y. Xu, and K. Tomsovic, "Bidding strategy for microgrid in day-ahead market based on hybrid stochastic/robust optimization," *IEEE Transactions on Smart Grid*, vol. 7, no. 1, pp. 227–237, Jan. 2016.



Xinchen Li received the B.S. degree in electrical engineering from Tianjin University, Tianjin, China, in 2022. His current research interests focus on microgrid operation and optimization.



Yixin Liu (M'22) received the B.S. and Ph.D. degree in electrical engineering from Tianjin University, Tianjin, China, in 2013 and 2018, respectively. He is currently an associate professor with Tianjin University. His research interests include the distribution system analysis and planning, energy management system of microgrid, and electricity power market.



Li Guo (M'11) received the B.Sc. and Ph.D. degrees in electrical engineering from the South China University of Technology in 2002 and 2007, respectively. He is currently a Full Professor with Tianjin University. His research interests include the optimal planning and design of microgrid, the coordinated operating strategy of microgrid, and the advanced energy management system.



hybrid ac–dc microgrid, and multi-terminal dc (MTDC) grids.

Xialin Li (M'15) received the B.Sc. and Ph.D. degrees from Tianjin University, Tianjin, China, in 2009 and 2014, respectively. In 2016, under the State Scholarship Fund, he was invited as a Visiting Professor to the Department of Electrical and Computer Engineering, University of Alberta, Edmonton, AB, Canada. Since 2018, he has been an Associate Professor with the School of Electrical Engineering and Automation, Tianjin University. His current research interests include the modeling and control of power converters, distributed generation,



generation system and microgrid, and power system security analysis. He was a recipient of the National Science Fund for Distinguished Young Scholars. He is the Chief Scientist of 973 project, “Research on the Key Issues of Distributed Generation Systems” from 2009 to 2013 that was participated by Chinese power engineering scientists from eight leading institutions.

Chengshan Wang (SM'11) received the B.Sc., M.Sc., and Ph.D. degrees from Tianjin University, Tianjin, China, in 1983, 1985, and 1991, respectively. He became a Full Professor with Tianjin University in 1996. He was a Visiting Scientist with Cornell University from 1994 to 1996 and as a Visiting Professor with Carnegie Mellon University from 2001 to 2002. In 2021, he was elected as an Academician of the Chinese Academy of Engineering, Beijing, China. His research is in the area of distribution system analysis and planning, distributed